# Very-High-Energy Heavy Ion Beam Dosimetry Using Solid State Detectors for Electronics Testing

Andreas Waets, Kacper Bilko, *Member, IEEE*, Andrea Coronetti, *Associate Member, IEEE*, Natalia Emriskova, Mario Sacristan Barbero, *Member, IEEE*, Rubén García Alía, *Member, IEEE*, Marco Durante, Christoph Schuy, Tim Wagner, Luigi Salvatore Esposito, Petteri Nieminen, and Uwe Schneider

***Abstract*— Very-high-energy (VHE), heavy ions are of particular interest for single event effects (SEEs) testing due to their combination of high linear energy transfer (LET) and high penetration within electronics components. The dosimetry of such beams poses an important challenge for facilities aiming to provide VHE ions for radiation effects testing. In this article, ion beam dosimetry using a silicon solid state detector is presented for uranium ions in the 100–1000 MeV per nucleon kinetic energy range. The study involves a combination of experimental measurements carried out at the SIS18 accelerator at Gesellschaft für Schwerionenforschung (GSI) and Monte Carlo (MC) simulation studies using FLUktuierende KAskade (FLUKA). Particular emphasis was put on the physical basis of interaction between both primary beam particles as well as secondary fragments, and the detector device. Our results demonstrate an excellent capability of understanding key beam properties and extracting the LET through comparison with simulation results. This benchmark study acts as a reference for developing and utilizing a heavy ion electronics testing infrastructure currently under development at Conseil Européen pour la Recherche Nucléaire (CERN).**

***Index Terms*— Conseil Européen pour la Recherche Nucléaire (CERN), FLUktuierende KAskade (FLUKA), Gesellschaft für Schwerionenforschung (GSI), Monte Carlo (MC) simulations, silicon detector, single event effects (SEEs), stopping and range of ions in matter (SRIM), very-high-energy (VHE) heavy ions.**

Manuscript received 29 September 2023; revised 21 November 2023, 7 December 2023, and 3 January 2024; accepted 3 January 2024. Date of publication 8 January 2024; date of current version 16 August 2024. This work was supported in part by EU-Funded Radiation Facility Network for the Exploration of Effects for Industry and Research (RADNEXT) Project, under Grant 101008126; and in part by the High-Energy Accelerators for Radiation Testing and Shielding (HEARTS) Project, Funded by the European Union under Grant 101082402, through the Space Work Program of the European Commission. *(Corresponding author: Andreas Waets.)*

Andreas Waets is with CERN, CH-1211 Geneva 23, Switzerland, and also with the Physik-Institut—Medical Physics and Radiation Research, University of Zurich, CH-8006 Zurich, Switzerland (e-mail: andreas.waets@cern.ch).

Kacper Bilko is with CERN, Université Jean Monnet, 42100 Saint-Étienne, France.

Andrea Coronetti and Mario Sacristan Barbero are with CERN, Institute d'Électronique et des Systèmes, Université de Montpellier, 34090 Montpellier, France.

Natalia Emriskova, Rubén García Alía, and Luigi Salvatore Esposito are with CERN, CH-1211 Geneva 23, Switzerland.

Marco Durante, Christoph Schuy, and Tim Wagner are with GSI, 64291 Darmstadt, Germany.

Petteri Nieminen is with the European Space Agency, 2201 AZ Noordwijk, The Netherlands.

Uwe Schneider is with the Physik-Institut—Medical Physics and Radiation Research, University of Zurich, CH-8006 Zurich, Switzerland.

Color versions of one or more figures in this article are available at https://doi.org/10.1109/TNS.2024.3350667.

Digital Object Identifier 10.1109/TNS.2024.3350667

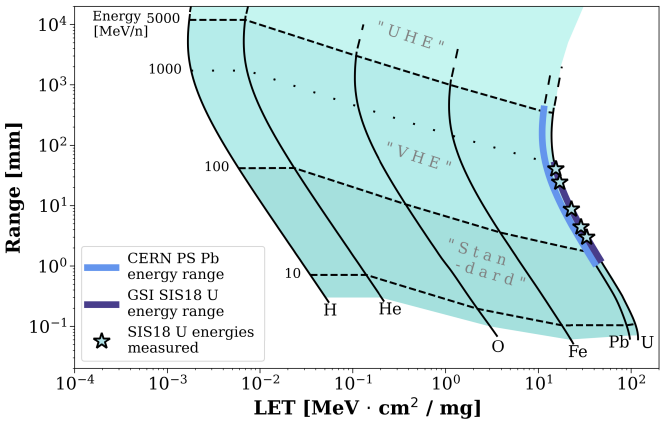


Fig. 1. Range versus LET in Si for different ions and energies. The different ion testing regimes (Standard, VHE, and UHE) are delineated as a function of the ion kinetic energy per nucleon. The energy range used at the CERN proton synchrotron (PS) and available energies at the GSI SIS18 accelerator are indicated, along with the primary $^{238}$U beam energies used in this work.

## I. Introduction

In THE beyond low Earth orbit (BLEO) space environment, both humans and mission-critical electronic components are continuously subject to galactic cosmic rays (GCR), which can cause detrimental effects. Generally peaking between 500 and 1000 MeV per nucleon (MeV/n) kinetic energy, the isotropic GCR flux consists of 85% protons, 14% helium nuclei and 1% heavier nuclei [1]. Despite their lower relative abundance, these heavy nuclei can be highly penetrating, undergo a significant amount of fragmentation, and deposit a large amount of energy. The main hazard from GCR radiation comes from stochastic interactions with tissue and electronics. This means that the probability of a subsequent macroscopic effect is proportional to the sustained dose, which is obtained as the convolution of the ion fluence (integrated flux) and the amount of energy transferred [2]. As generally adopted within the radiation effects community, the linear energy transfer (LET) is used to quantify this amount, expressing the deposited energy in matter per unit path length in units of keV/$\mu$m or MeV cm$^2$/mg, when weighted by the target material density. The resulting dose $D$, or energy deposited per unit mass, to a test object can then be quantified as the product of the LET of a beam of energy $E$, and the fluence $\Phi$ in units of cm$^{-2}$

$$D(E, \Phi) = \mathrm{LET}(E) \times \Phi. \tag{1}$$

The probability of an electronic component failure or error induced by a single particle, also called a single event effect (SEE), is quantified by the SEE cross section as a function of the LET. For this reason, the LET is a primary figure of merit for testing electronics; when using ion beams, it can be varied by tuning the kinetic energy of the beam or changing the ion species [3]. In Europe, several facilities use different heavy ion species at so-called standard energies (around tens of MeV/n) for electronics testing. As shown in Fig. 1, ions at these energies have a limited penetration depth within silicon. Higher energy beams between 100 and 5000 MeV/n, i.e., within the so-called very-high-energy (VHE) range, are more representative of inducing radiation effects caused by GCRs and are also exceptionally appealing for testing due to their combination of high LET and high penetration within electronic components. A penetration depth above 1 mm is desirable to ensure that the beam reaches all sub-layers of a device under test and that the LET in these layers can be kept as constant as possible. This is of particular importance for testing state-of-the-art microelectronic components with complex, 3-D architectures, and board-level testing. The current development of a VHE ion testing facility at Conseil Européen pour la Recherche Nucléaire (CERN) using lead ($^{208}$Pb) ions is motivated by the limited VHE ion availability in Europe and worldwide and relies on past experience using ultrahigh-energy (UHE) 150 GeV/n $^{208}$Pb ions in the super proton synchrotron (SPS) North Area [4], [5]. Accurate dosimetry is essential when characterizing and measuring quantities such as the ion fluence and the beam quality (LET of a particular ion species); it is one of the key challenges for high-energy heavy ion testing. Within the radiation effects community, generally, an error up to 10% on the energy or the LET is accepted [6]. This article describes the experimental verification of CERN's envisaged VHE ion dosimetry technique, using a silicon diode detector measuring energy deposition as a means of verifying the beam energy. In addition, it explains the attempted beam energy degradation and full fragmentation methods using passive degrader slabs. The CERN heavy ion activity is carried out using similar ion beams as present in the SIS18 accelerator at Gesellschaft für Schwerionenforschung (GSI). Test preparation and in-depth characterization of the beams were aided by computational tools such as the Monte Carlo (MC) code FLUktuierende KAskade (FLUKA) [7], [8] and stopping and range of ions in matter (SRIM) [9], which are key in explaining features of the experimental energy deposition spectra and calculating the associated LETs.

The article is organized as follows. Section II describes the GSI accelerator facility and ion beams used. The experimental setup and data are discussed in Section III, and the FLUKA simulation setup and results are shown in Section IV. Experiment and simulation are correlated in Section V, followed by a summary and outlook in Section VI.

## II. Description of Facility and Beams

GSI has a large variety of heavy ions at its disposal, elements ranging from hydrogen to uranium can be extracted from either of the ion sources [10]. The linear UNILAC accelerator generally injects the ions at 11.4 MeV/n into the SIS18 synchrotron for further acceleration to relativistic energies. Upon prior request, any beam energy within the 50 to 1000 MeV/n range could be selected. Only uranium ions were used in this experiment, for which the energies were chosen to cover a representative set of beam LETs for SEE testing (as summarized in Table I) by using SRIM. The similarity of U (Z = 92, A = 238) and Pb (Z = 82, A = 208) ions, also displayed in Fig. 1, allows to use this experiment as benchmark of the envisaged dosimetry approach for the CERN VHE heavy ion activity. $^{238}$U beams were accelerated in a charge state of $73^+$ but were fully stripped when exiting the vacuum window in GSI's high-energy irradiation experimental facility Cave A, where the test campaign took place. Over the course of the testing activity, beams were extracted in spills with a 3 to 4 s duration and a similar time gap in between. During the majority of the measurements, magnetic raster scanning of the beam was enabled, sweeping a 1 cm FWHM Gaussian beam over a $2 \times 2\,\text{cm}^2$ area in 1 mm steps or spots. The width (FWHM) of the beam was set to be a multiple of scan spot distance to ensure a homogeneous flux on target by superimposing Gaussian profiles. With the scanning focal point located 13 m upstream, we could assume a parallel beam at the test location. The number of ions per beam spot was monitored by an ionization chamber (IC) beam monitor directly downstream of the vacuum window, converting monitor pulses to a particle fluence [11]. The IC calibration was carried out using a 1 mm thick BC400-like scintillator before and during the test campaign. The facility reported averaged fluxes on the order of $10^2$ and $10^4$ ions/cm$^2$/s in each spill. Primary beam parameters used during the campaign are summarized in Table I.

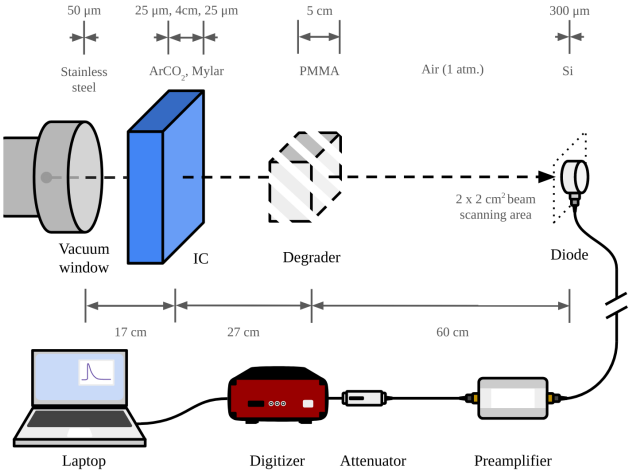


Fig. 2. Schematic of the experimental setup, showing the different components, their relative distances, thickness and composition. The data acquisition chain shown below was placed directly next to the test station in Cave A at GSI. The PMMA degrader was only used for a few dedicated runs at 800 MeV/n $^{238}$U energy.

## III. Experimental Setup and Diode Measurement Results

### A. Diode Test Setup in Cave A

A schematic representation of the test setup in Cave A is shown in Fig. 2. An IC that allowed us to estimate the

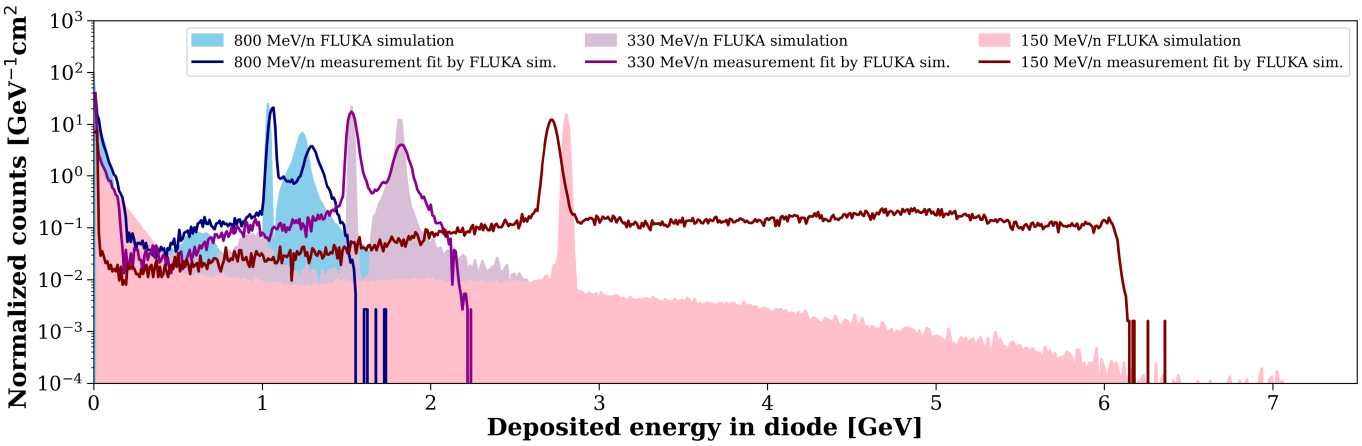


Fig. 3. Energy deposition spectra measured by the Si diode for 800, 330, and 150 MeV/n $^{238}$U beams (solid lines). The shaded areas represent the results from FLUKA simulations. For both measurement and simulations, the values are normalized by the fluence and bin width (10 MeV). Measurements were scaled according to the linear measurement versus simulation dependence shown in Fig. 8 and detailed in Section V.

beam flux was placed directly downstream of the 50 $\mu$m-thick steel vacuum window. The IC consists of two cathode planes symmetrically arranged around a single anode plane with a gap of 10 mm in between. The cathodes and anode are made of a nickel-coated polyester mesh and the IC contains a mixture of two gases, 80% argon and 20% $CO_2$ with an overall density of 1.8 mg/cm$^3$. The housing of the IC is made from aluminum and has two 25 $\mu$m thick metalized Mylar windows for the beam to pass through. The 300 $\mu$m-thick Si diode (Canberra, model: FD 50-14-300 RM) was placed at 1 m distance to accommodate space for supports of polymethylmethacrylate (PMMA) degraders (5 and 6.2 cm thickness) and other electronic components tested during the campaign; these were placed out of the beam during the dedicated diode measurements. This particular diode setup was chosen for its simplicity and representativeness in understanding the physical basis of radiation effects in electronics, measuring energy deposition in its active Si layer on an event-by-event basis. In addition to this, it can be deployed to measure test beams in a parallel or noninvasive way to other components under test simultaneously. The diode is housed in a metallic case, which partially encloses the active sensitive surface area. The 0.5 cm$^2$ exposed detection surface and the metallic case were fully covered by the magnetic scanning area. The case itself was further enveloped by a 30 $\mu$m aluminum foil to shield the (photosensitive) diode from light. Given the low ion fluxes and consequently low activation levels, the full readout system (including a remotely controlled laptop) could be placed directly next to the beam inside the cave. The diode itself was operated at full silicon depletion using a 60 V reverse bias; the signal was amplified using a Cividec C1-HV 20 dB current-sensitive preamplifier (certified gain $G_{\mathrm{PA}}$ of 21.9 dB). During the first checks with 150 MeV/n energy beams, energy deposition events outside of the digitizer (1 GS/s Caen model DT5751) 1 V input dynamic range were recorded. For this reason, a 6 dB attenuator was placed in the readout chain between the preamplifier and the digitizer. The Caen WaveDump software was used to collect the data during measurements; these were post-processed to remove pile-up events and extract the deposited energy in the diode as the integrated amount of charge in each pulse. We adopted the 3.6 eV average energy required to create one electron-hole pair in silicon, denoted as $\epsilon_{\mathrm{eh}}$. Taking into account all components of the readout chain, the energy deposited $\epsilon_{\mathrm{dep}}$ by a single event is equal to the total charge, i.e., the integral of the current pulse $\int I(t)dt$ times energy needed to create one electron-hole pair

$$\epsilon_{\mathrm{dep}} = \frac{\epsilon_{\mathrm{eh}}}{e}\int I(t)dt = \frac{\epsilon_{\mathrm{eh}}}{e}\int \frac{V(t)}{(G_{\mathrm{PA}} - |A|)R \cdot ADC}dt \qquad (2)$$

with $e$ the electric charge, $A$ the (compound) attenuation value which also takes into account the contribution from cables and connectors, $R$ the preamplifier input resistance (50 Ω), and $ADC$ the number of digitizer channels. It is important to note that uncertainties on the different factors in (2) can propagate into an inaccurate energy deposition calculation. Technically, $\epsilon_{\mathrm{eh}}$ needs to be corrected by a calibration factor, which for this diode was carried out using several ions in the standard energy range. However, any result from a calibration measurement is of limited value since the ion kinetic energies per nucleon and associated deposited energies considered in this study are two orders of magnitude higher, potentially affecting the charge collection within the Si active layer, These effects have already been studied using heavy ions and have shown to affect the calibration procedure [12]. Another source of uncertainty stems from the inherent attenuation of the cabling and connectors, despite the advantage of using short cables due to the proximity of the readout electronics to the diode setup itself. The 6 dB attenuator lacks a certified value provided by the manufacturer and is signal frequency dependent. As can be expected from commercially available components, a 10% deviation from this value is possible. The use of a single effective attenuation value was chosen to analyze the digitized event pulses of all measurements, accounting for the aforementioned effects on the obtained signals but keeping $\epsilon_{\mathrm{eh}} = 3.6$ eV fixed, this will be further detailed in Section V.

TABLE I

PRIMARY $^{238}$U BEAM CHARACTERISTICS AND MEASURED FLUENCES BY THE SILICON DIODE SETUP

| Selected beam properties | | Diode measurements |
|---|---|---|
| Beam kinetic energy [MeV/n] | $LET_{SRIM}$ [MeVcm$^2$/mg] | Total fluence [$\times 10^5$ cm$^{-2}$] |
| 150 | 33.0 | 1.72 |
| 190 | 28.8 | 4.20 |
| 330 | 21.8 | 3.59 |
| 600 | 17.2 | 1.91 |
| 800 | 15.7 | 3.02 |
| 800* | / | 1.23 |
| 800† | / | 2.27‡ |

∗ 5 cm thickness PMMA energy degrader in-beam.
† 6.2 cm thickness PMMA fragmenter in-beam.
‡ Obtained counting all fragments measured by diode.

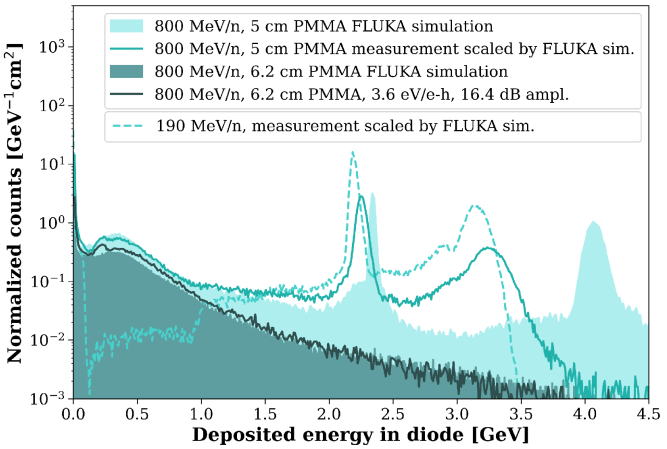


Fig. 4. Energy deposition spectra measured by the Si diode for an 800 MeV/n $^{238}$U beam degraded by 5 and 6.2 cm of PMMA. The shaded area represents the result from the FLUKA simulation. For comparison, the 190 MeV/n measurement is also shown. For both measurements and simulations, the values are normalized by the fluence and bin width (10 MeV). Measurements were scaled according to the linear measurement versus simulation dependence shown in Fig. 8 and detailed in Section V except for the fully fragmented case: due to the absence of a primary peak the scaling is not applicable.

### B. Diode Measurements

A representative subset of all acquired energy deposition spectra is shown in Fig. 3 as solid lines for three energies: 800, 330, and 150 MeV/n. To obtain these, the effective amplification was set to 16.4 dB. Based on the FLUKA results presented in Section IV, this implies that the actual attenuation was 5.5 dB instead of 6 dB. Three main features motivated the more detailed MC simulation studies after the test: 1) a clearly visible cutoff at around 6 GeV deposited energy in the 150 MeV/n spectrum [as shown in Fig. 3(c)]; 2) the presence of a lower amplitude, secondary peak at higher deposited energy than the sharper primary peak in all measurements except in the 150 MeV/n spectrum [as shown in Fig. 3(a) and(b)] and finally; and 3) a continuous distribution of events between zero and peak primary deposited energy. In addition, a large amount of low energy deposition events is present in all spectra and in a few cases even exceeds the primary energy deposition peak. This region of the spectrum is partially subject to the detection threshold setting on the digitizer which was adjusted between different measurements.

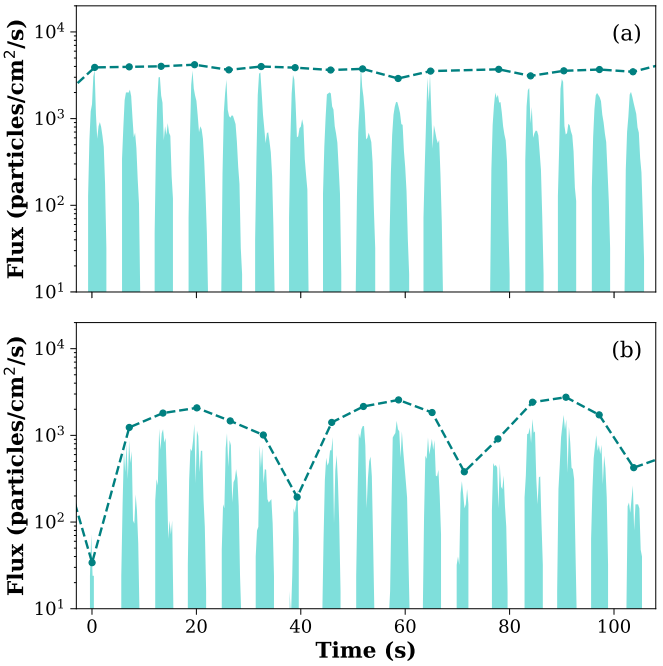


Fig. 5. Flux profiles recorded for 150 MeV/n $^{238}$U ions (a) without magnetic scanning and (b) with magnetic scanning. The dot markers indicate an integrated flux of all events for each spill and therefore give a value in units of [particles/cm$^2$].

As a result noise signals could be counted as actual energy deposition events.

The measurements at 800 MeV/n primary energy shown in Fig. 4 entail that placing a 5 cm stack of PMMA plates in the beam path degrades the beam energy in such a way that the primary energy deposition peak increases by more than 1 GeV (by comparison with Fig. 3). From this, we can infer that also the associated (degraded energy) beam LET is higher. The spectrum closely resembles that of the 190 MeV/n case, indicating that degraders can be used for this type of beam to achieve any desired resulting primary energy and associated LET if the thickness of the degrader can be chosen precisely. This approach is used in particle therapy centers [13] and in dedicated facilities such as the NASA Space Radiation Laboratory [14], [15] in the USA. In addition, placing a 6.2 cm stack of PMMA plates fully fragments the primary beam as also shown in Fig. 4. Both measurements using PMMA degraders validate the test preparation approach of estimating the primary beam range using SRIM. All these features will be further commented on when discussing the comparison with FLUKA simulation results in Section IV-B.

As shown in Fig. 5(a) for a time period without magnetic scanning, the diode was able to resolve the spill time structure of the beam in a clear way, thanks to its ability to register on an event-by-event basis provided that the flux is low (up to $10^4$ ions/cm$^2$/s). In a few cases, there was no exact correspondence between the length of a spill and the length of a scan, causing a modulation of the flux shown in Fig. 5(b), due to the fact that the scanning area is larger than the active area of the diode. The diode acquisition time corresponded precisely to the requested amount of scans at the start of each measurement. By counting the number

of primary events through direct exposure, the diode could estimate the fluence. This was done by using the integral values of the pulses. Only events were used for which pulses were actually recorded, excluding false triggers. Also pile-up events and pulses not returning to baseline before the end of the acquisition frame (partially acquired or nonconverging pulses) were not taken into account. This procedure results in an average 10% rejection of pulses for all measurements. Using the pulse integral spectrum, the primary peak could be identified. Complete deconvolution from the secondary peak and background is however not straightforward: as will be discussed in Section IV-B, an overlap with the nondirect exposure event distribution exists. Combined with the detector resolution, it can be expected that the counts in the primary peak are systematically overestimated, despite the rejection of events as described above. Pulses within $2\sigma$ from the peak integral value were counted as direct exposure primary particles, the error on this value can be between 20% and 30% based on the considerations made above. Using these counts, the fluence values given in Table I were calculated using the $0.5\,\mathrm{cm}^2$ nonexposed diode surface area. The 10% uncertainty on the radius can propagate to an additional $\pm 20\%$ on the listed total fluence values. Fragmentation and scattering processes drastically reduce the fluence recorded by the diode when using either of the two PMMA degraders.

## IV. MC Simulations of Energy Deposition

### A. Simulation Setup

During experiment preparation, the expected LETs (calculated using SRIM v2013) and energy deposition spectra (simulated using FLUKA) as a function of particle type and energy were obtained. The general purpose MC code FLUKA [7], [8] is a most suitable tool in this regard, regularly used in accelerator environments and extensively benchmarked on a microscopic level [7], [16], [17]. Detailed simulations, involving either a simplified diode model with just a single Si layer, or a Cave A-like geometry where the FLUKA model accurately represents the test conditions as described in Section III, have allowed to run multiple configurations prior to the experiment. For simplicity, the anode and cathode meshes in the IC were not explicitly modeled. Any beam fragmentation upstream of the vacuum window was deemed negligible, i.e., the beam was modeled to be pure $^{238}$U ions in a 92+ charge state. In combination with SRIM, the thickness of the PMMA degrader was chosen to be 5 cm, aimed at degrading the primary beam energy through electronic stopping power (dE/dx). The in-depth analysis of the measured spectra through simulations after the experiments proved to be a decisive tool in providing a more fundamental and in-depth description of the beam. All calculations in FLUKA were carried out in versions 4.2 and 4.3, including consistency checks between the two.

In the user-defined simulation settings, full ion transport was requested, including models for spallation processes such as fission and fragmentation, which at these energies can take place as a result of inelastic interactions of the primary beam with any material in its path [18], [19] These materials include the vacuum window, IC, degrader but also the diode casing itself. Nucleus-nucleus collisions in the VHE ion regime are handled in FLUKA through an extensively modified Relativistic Quantum Molecular Dynamics Model (RQMD) model [20], [21], [22]. Subsequent fragment de-excitation (evaporation, fission, Fermi break-up) is performed in the cascade-preequilibrium PEANUT event generator [23]. In the scope of space radiation studies, heavy ion transport and interactions in FLUKA have been well benchmarked against experiments in the energy range considered in this study [24], [25], [26], [27]. The computationally heavy electromagnetic sector processes were enabled down to 150 keV, allowing to track energetic delta ray electrons emerging from the ion tracks and potentially depositing energy in a larger volume. For reference, the ESTAR database [28] indicates a range of more than 150 $\mu$m in silicon for 150 keV electrons. At simulation initialization, stopping power tables were printed for the primary particles, distinguishing between unrestricted dE/dx and restricted dE/dx which takes into account the delta ray production threshold. For all energies used at GSI, the difference between the two amounted to less than 10%. A summary of the beam and physics settings is given in Table II. Resulting physical quantities were obtained through event-by-event energy deposition scoring in material regions and double-differential yields of particles when crossing region borders within the model.

TABLE II
Settings Used for FLUKA Simulation Studies

| | |
|---|---|
| **Beam properties** | |
| Species | Uranium (Z=92, A=238) |
| Size [cm$^2$] | $2 \times 2$, uniform |
| Energy [MeV/n] | 150 - 800 |
| Dispersion [MeV/n] | 0.0 |
| **Physics settings** | |
| Transport thresholds: | |
| - electrons, positrons, photons | 150 keV |
| - hadrons | 1 keV |
| - neutrons | 0.01 meV |
| Ion transport settings: | Full transport + spallation physics enabled |

### B. FLUKA Simulation Results

The points addressed first are the most prominent features in the energy deposition spectra as discussed in Section III-B. To first order, the maximal energy deposited in a material can be estimated using SRIM. For a given primary energy, this is calculated as the product of the stopping power and the mean path length of the particles in the sensitive volume. For $^{238}$U ions in a 300 $\mu$m-thick Si layer this corresponds to 30 MeV/n. In FLUKA, ions were launched at a very tiny Si target (<1 mm) with an unrealistically large energy dispersion (100%) at energies just above and below 30 MeV/n. As shown in Fig. 6, a cutoff at around 7 GeV deposited energy is seen. The higher LET for 20 MeV/n compared to 30 MeV/n does not result in a maximal energy deposition since the range is considerably smaller than 300 $\mu$m. On the other hand, the LET of a 40 MeV/n is lower than for 30 MeV/n

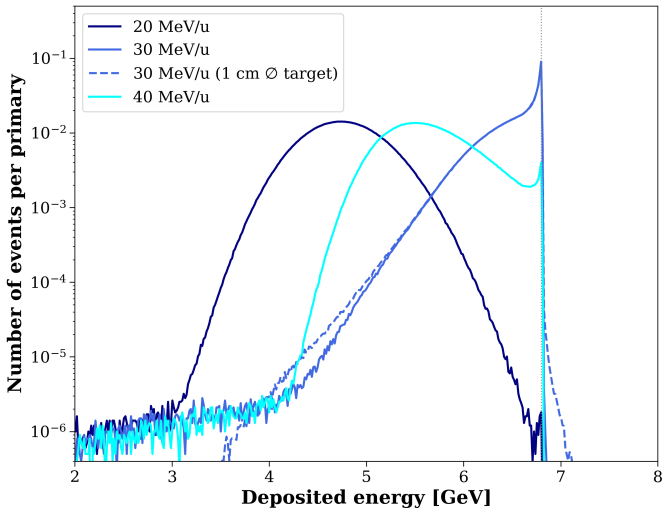


Fig. 6. FLUKA simulations of the energy deposition in a 300 $\mu$m thick, 0.1 mm radius Si target with $^{238}$U ions. To all primary beam energies, a beam energy dispersion of 100% was applied to probe the maximum possible energy deposition in a 300 $\mu$m Si layer by $^{238}$U ions.

and only deposits its energy only partially since the range is larger than 300 $\mu$m. These observations confirm the presence of a maximum energy deposition cutoff in the 150 MeV/n spectrum as shown in Fig. 3(c). Only in this measurement, beam particles are degraded down to 10 s of MeV/n, resulting in this observation. When simulating using a more realistic size of the target (1 cm diameter shown by the dashed line in Fig. 6), scattering effects become present which can make this cutoff less sharp.

The origin of the smaller, secondary peak is explained by scoring the LET of individual particles. This is shown in Fig. 7 for 330 MeV/n which is representative for all other energies. Ions traversing the diode case which partially covers the active Si layer lose energy, by a consequence have a higher LET and deposit more energy. The secondary peak is absent in the 150 MeV/n spectrum since the primary particles do not penetrate the casing layers. A small yield of LET above the primary peak is observed: these result from interactions with the edge of the case but were still counted as direct exposure events. A deconvolution of the LET distribution arriving at the diode as a function of particle charge Z is shown in the bottom part of Fig. 7. As typically described in radiation effects studies, we can make the distinction between "projectile-like" fragments or "target-like" fragments as products of heavy-ion fragmentation reactions [29]. Not necessarily all generated fragments are counted in the simulation due to the small solid angle of the diode detector. The distinction between target- and projectile-like is set to Z = 28 which corresponds to the heaviest constituent (Ni) of the stainless steel material implemented in the FLUKA model. Heavy, projectile-like fragments are created with a continuous distribution of LETs up to the primary peak through evaporation or Fermi-breakup reactions [30], [31]. The reaction products are generally a multitude of light particles (neutrons, hydrogen-like, helium-like) populating the low-LET region and a distinct, single heavy constituent with a lower Z but roughly the same kinetic energy per nucleon as the primary beam particles.

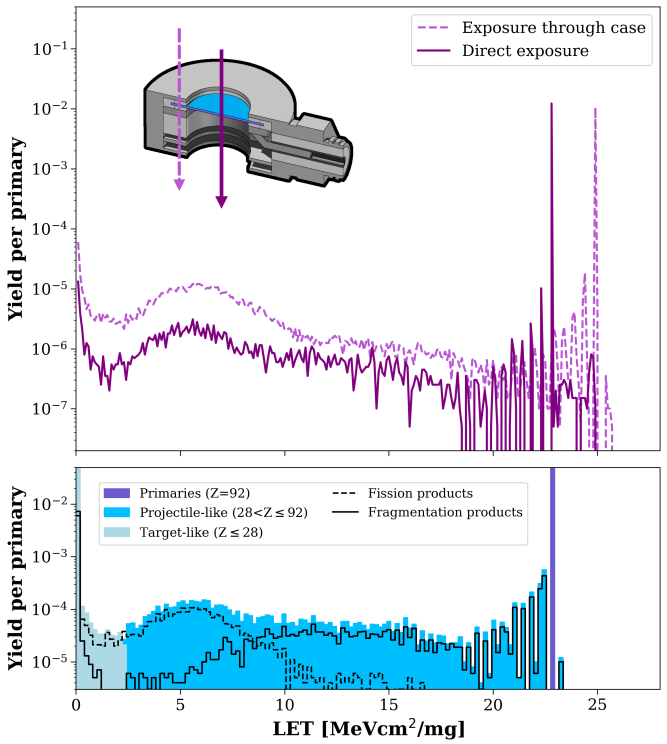


Fig. 7. FLUKA simulations of the LET (top) of 330 MeV/n $^{238}$U beam particles arriving at the diode and their particle disentanglement (bottom). The insert shows the FLUKA simulation model of the diode which was embedded into the GSI setup model described in Section IV-A (Al foil not shown for visualization purposes). The two curves distinguish the LET of beam particles traveling through the case (dashed) and directly hitting the active Si area of the diode (solid). The bottom plot disentangles primary, target-like and projectile-like particles and indicates if the products result from a fission or fragmentation inelastic nuclear interaction.

The proportionality of the LET to $Z^2$ [32] is clearly visible just below the primary peak; this modulation of the distribution is not seen in the measured spectra as a result of the diode detector's limited resolution with respect to the idealized simulation setup. A local maximum of projectile-like fragments is present at around 5 MeVcm$^2$/mg and is mostly populated by fission products. These are discriminated based on the presence of two daughter nuclei similar in mass and energy with an atomic number Z around or below half that of the primary $^{238}$U ions, accompanied by a limited amount of light particles. The resulting energy deposition peak at around half the primary energy peak is shown in Fig. 3 and present for all spectra between 190 and 800 MeV/n. The surplus in the distribution at 0 MeVcm$^2$/mg is due to a large number of neutrons which can impact neighboring test devices or ancillary electronic equipment [33]. The fragment yield in the LET distribution increases when particles travel through the case. Subsequent inelastic interactions within the Si active layer itself contribute to the energy deposition spectrum as well.

The simulated energy deposition spectra for the same energies as the diode measurements are shown in Figs. 3 and 4. From the simulation results, the error on the peak values is limited to less than 5%. Qualitatively, the FLUKA results show a satisfactory agreement with the measurements for all

primary energy deposition peaks; in addition, general features in the profiles, such as the low energy peak and intermediary fragment distribution are well represented. The agreement in the 5 cm degrader case is very good up to the primary peak; in the fully fragmented beam measurement, the correspondence is excellent. The simulation results are virtually insensitive to enabling or disabling EMF particles (photons, electrons, and positrons). Among the main discrepancies is the overall shape of the secondary peaks in all spectra. This observation and the inability to match both the primary energy deposition peak and maximum energy cutoff in the 150 GeV/n simultaneously can be mainly attributed to inaccuracies in the diode simulation model: the exact structure and material composition is proprietary information. In addition, the Si layer thickness could deviate away from 300 $\mu$m to allow a significant difference in results. The effect on the energy deposition is, however, expected to be limited, the effect of the $\pm$ 10 $\mu$m uncertainty on the thickness is obscured by the width of the primary peak. The other key point to take into account here is the transition between the RQMD model and a Boltzmann Master Equation model in FLUKA which happens at 150 MeV/n. On the simulation side, there is an inherent level of uncertainty of using a single MC code to calculate particle energy loss, range, and fragmentation yields. At the end of the particle range, the variability of the LET is large and difficult to quantify: a considerable challenge in (micro-)electronics testing of novel components for which the composition is not accurately known [34].

## V. Discussion

Measurements of energy deposition provide only an indirect means of determining the primary beam energy in the VHE range we consider here. To pin down this value and extract the associated beam LET, simulations are required. In addition, due to the large range of delta ray electrons emerging from the ion track, the diode cannot experimentally determine the full energy deposition and therefore measures restricted LET. In the preceding sections, the measurements and simulation results for the test campaign at GSI have been compared in a qualitative way; the correlation needs to be made on a quantitative basis with a limited amount of parameters that are fixed for all primary energy cases studied. The approach used here was to use the results from a single FLUKA simulation setup in terms of beam physics settings, geometric model, and scoring, only varying the primary beam energy. To process all measurements, a single, effective signal amplification value was chosen to best fit the simulation spectra. We limited ourselves to the comparison of the primary energy deposition peaks, given the uncertainties on the diode simulation model which affect the secondary peaks; also the maximum energy deposition cutoff was not considered here. The result of this procedure shown in Fig. 8 indicates that an amplification of 16.4 dB (i.e., the specified amplification means an attenuation of 5.5 dB) for the measurements show an excellent fit to the simulation data with slope 1 and small intercept. For comparison also the result for 6 dB is shown, presenting considerably worse fit parameters.

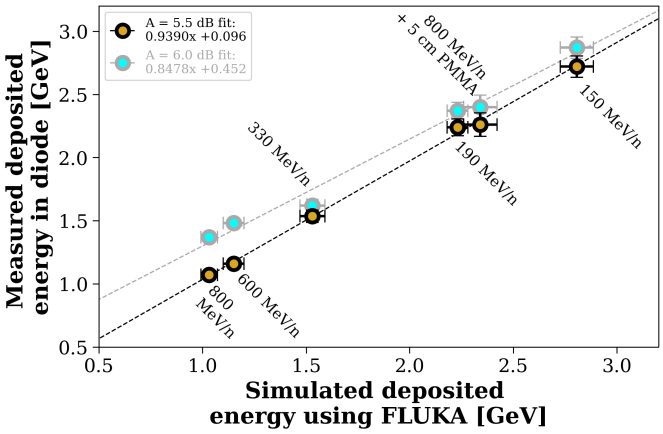


Fig. 8. Simulated versus measured primary peak energy deposition values and a linear fit of the data points (dashed line) for an attenuation value of 5.5 and 6 dB. The error bars indicate the peak FWHM for both simulation and measurement.

The objective of this study was met since a match between MC simulations and measurements was achieved to extract the beam LETs shown in Fig. 9, despite the uncertainties on both experimental and simulation side. Using a first-order approximation, the restricted LET can be extracted also from the measurements, provided the assumption that the energy deposition is constant over the thickness of the silicon layer. Given the much larger deposited energy by the primary ions over the delta ray electrons, the restricted LET should be very close to the unrestricted LET, as was also confirmed by simulation results given in Fig. 9. As shown in the same figure, the agreement between the LETs extracted from simulations and measurements is very good given the generally accepted 10% uncertainty margin in the radiation effects community. The accuracy of the extracted LET, however, becomes questionable closer to the Bragg peak or when the size of the sensitive volume is uncertain, again highlighting the need for simulation codes as detailed in heavy ion testing standards [35]. In this procedure, the choice for the FLUKA simulations as "ground truth" was essential but justified given the larger number of possible errors in the measurements and the extensive benchmarking of VHE heavy ion models in FLUKA with experiment. This result shows that we can use this approach with similar ions in CERN's VHE ion testing facility, which will accommodate $^{208}$Pb beams in the same energy and LET range as discussed in this work. Calculations with SRIM also show that within this energy range the penetration depth of particles in silicon is larger than 1 mm, as desired to cross all layers of modern microelectronic components with heavy ions. In CERN's VHE ion activity, the potential sources of error in the dosimetry method discussed here will be subject to further investigation. On the experimental side, the uncertainties on the diode calibration factor and resulting signal attenuation can be improved; for example, by simplifying the readout chain from a combination of amplifier and attenuator to the use of a bias tee, given that the energy deposition signals are large enough. The measurement vs. simulation approach is subject to the diode's energy resolution which could deteriorate over

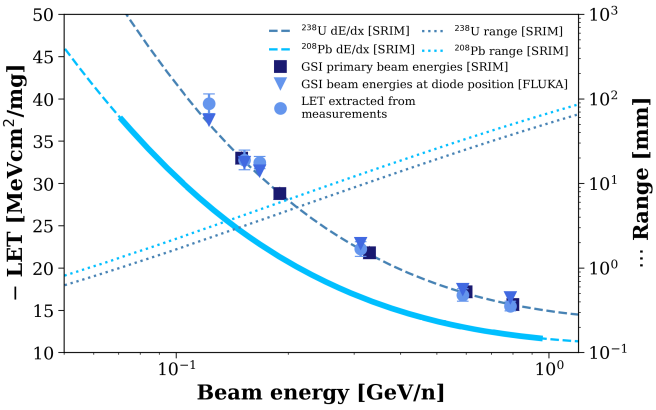


Fig. 9. LET as a function of beam energy extracted from SRIM for the $^{238}$U primary beam energies. The triangle markers indicate the LET values extracted from the simulation and correspond to the beam energies arriving at the diode (including the 800 MeV/n + 5 cm PMMA case). For comparison, at the same energies as for the simulations the (restricted) LET extracted from measurements are shown. The dotted lines indicate the range of the ions in Si, as a function of beam energy on the right axis. The thick blue line indicates the energy range of operation envisaged in CERN's VHE ion facility with $^{208}$Pb ions.

time as a result of sustained irradiation damage and therefore needs to be monitored [36]. On the simulation side, the uncertainty on the LET (particularly at the end of particle range at low energy) and resulting deposited energy could be partially mitigated by comparison to other MC codes. This argument holds for differences in implemented nuclear physics models as well which calculate the beam fragmentation yields and have important implications for SEE testing [37]. As shown here, the emphasis will need to be on fragmentation yields which can explain differences between simulation and measurement, despite the complete fragmentation case showing a near-perfect agreement. Accurate knowledge of beam fragmentation is very important in light of developing and optimizing CERN's heavy ion facility, considering the amount of nonvacuum material (air, beam instrumentation) that needs to be traversed. These calculations can clarify if the use of passive degraders as demonstrated in this work is desirable or not. In addition, considerable attention will need to be given to calibrating the beam line instrumentation to achieve accurate flux readings. A collimator or mask with a well-defined opening can be used that allows suppression of the secondary, degraded energy peak present for this diode architecture. The accurate knowledge of the mask opening area can also limit the uncertainty on the extracted beam flux and fluence.

## VI. Conclusion

In this study, it has been shown that the combination of a silicon diode with MC simulations forms a suitable tool for dosimetry of VHE ion beams if measurement and simulation uncertainties can be narrowed down. The measurements indicate its ability to register individual particles on an event-by-event basis and can resolve heavy ion beam spill structures, provided that the particle flux is low. Measurements of energy deposition spectra showed a satisfactory agreement with FLUKA simulations, which are required to obtain the primary particle LET with confidence. In addition, the same satisfactory agreement was found between simulation and measurement of a PMMA degrader configuration, in which the primary beam energy was degraded to yield a higher LET. The complete fragmentation of the primary beam was also demonstrated, yielding interesting opportunities for radiation hardness assurance applications [38]. The gathered experience from this study will be used for the development of a VHE ion radiation effects testing facility at CERN.

## References

[1] J. A. Simpson, "Introduction to the galactic cosmic radiation," in *Composition and Origin of Cosmic Rays*, M. M. Shapiro, Ed. Dordrecht, The Netherlands: Springer, 1983, pp. 1–24.
[2] M. Durante and F. A. Cucinotta, "Physical basis of radiation protection in space travel," *Rev. Modern Phys.*, vol. 83, no. 4, pp. 1245–1281, Nov. 2011.
[3] K. A. LaBel et al., "Single event effect proton and heavy ion test results for candidate spacecraft electronics," in *Proc. Workshop Rec. IEEE Radiat. Effects Data Workshop*, Tucson, AZ, USA, Jul. 1994, pp. 64–71.
[4] R. G. Alía et al., "Ultraenergetic heavy-ion beams in the CERN accelerator complex for radiation effects testing," *IEEE Trans. Nucl. Sci.*, vol. 66, no. 1, pp. 458–465, Jan. 2019.
[5] M. Kastriotou et al., "Single event effect testing with ultrahigh energy heavy ion beams," *IEEE Trans. Nucl. Sci.*, vol. 67, no. 1, pp. 63–70, Jan. 2020.
[6] *Single Event Effects Test Method and Guidelines*, Standard 25100, 2014.
[7] C. Ahdida et al., "New capabilities of the FLUKA multi-purpose code," *Frontiers Phys.*, vol. 9, Jan. 2022, Art. no. 788253.
[8] G. Battistoni et al., "Overview of the FLUKA code," *Ann. Nucl. Energy*, vol. 82, pp. 10–18, Aug. 2015.
[9] J. F. Ziegler, M. D. Ziegler, and J. P. Biersack, "SRIM—The stopping and range of ions in matter (2010)," *Nucl. Instrum. Methods Phys. Res. Sect. B, Beam Interact. Mater. At.*, vol. 268, nos. 11–12, pp. 1818–1823, Jun. 2010.
[10] W. Barth, R. Hollinger, A. Adonin, M. Miski-Oglu, U. Scheeler, and H. Vormann, "LINAC developments for heavy ion operation at GSI and FAIR," *J. Instrum.*, vol. 15, no. 12, Dec. 2020, Art. no. T12012.
[11] F. Luoni et al., "Beam monitor calibration for radiobiological experiments with scanned high energy heavy ion beams at FAIR," *Frontiers Phys.*, vol. 8, Sep. 2020, Art. no. 568145.
[12] B. D. Wilkins, M. J. Fluss, S. B. Kaufman, C. E. Gross, and E. P. Steinberg, "Pulse-height defects for heavy ions in a silicon surface-barrier detector," *Nucl. Instrum. Methods*, vol. 92, no. 3, pp. 381–391, Apr. 1971.
[13] J. M. Schippers, "Beam transport systems for particle therapy," in *Proc. CERN Accel. School, Accel. Med. Appl. (CAS)*, Jun. 2017, pp. 241–252.
[14] C. La Tessa, M. Sivertz, I.-H. Chiang, D. Lowenstein, and A. Rusek, "Overview of the NASA space radiation laboratory," *Life Sci. Space Res.*, vol. 11, pp. 18–23, Nov. 2016.
[15] L. C. Simonsen, T. C. Slaba, P. Guida, and A. Rusek, "NASA's first ground-based galactic cosmic ray simulator: Enabling a new era in space radiobiology research," *PLoS Biol.*, vol. 18, no. 5, May 2020, Art. no. e3000669.
[16] H. H. Braun, A. Fassò, A. Ferrari, J. M. Jowett, P. R. Sala, and G. I. Smirnov, "Hadronic and electromagnetic fragmentation of ultrarelativistic heavy ions at LHC," *Phys. Rev. Special Topics Accel. Beams*, vol. 17, no. 2, Feb. 2014, Art. no. 021006.
[17] G. Battistoni et al., "The FLUKA code: Description and benchmarking," in *Proc. AIP Conf.*, Mar. 2007, pp. 31–49.
[18] A. Lechner, "Particle interactions with matter," in *Proc. CERN Yellow Rep. School*, Dec. 2018, pp. 47–67.
[19] K. S. Krane, *Introductory Nuclear Physics*. New York, NY, USA: Wiley, 1988.
[20] H. Sorge, H. Stöcker, and W. Greiner, "Poincaré invariant Hamiltonian dynamics: Modelling multi-hadronic interactions in a phase space approach," *Ann. Phys.*, vol. 192, no. 2, pp. 266–306, Jun. 1989.
[21] H. Sorge, H. Stöcker, and W. Greiner, "Relativistic quantum molecular dynamics approach to nuclear collisions at ultrarelativistic energies," *Nucl. Phys. A*, vol. 498, pp. 567–576, Jul. 1989.

[22] H. Sorge, "Flavor production in Pb(160AGeV) on Pb collisions: Effect of color ropes and hadronic rescattering," *Phys. Rev. C*, vol. 52, no. 6, pp. 3291–3314, Dec. 1995.

[23] G. Battistoni, F. Cerutti, A. Ferrari, J. Ranft, S. Roesler, and P. R. Sala, "Hadron production simulation by FLUKA," *J. Phys., Conf. Ser.*, vol. 408, Feb. 2013, Art. no. 012051.

[24] G. Battistoni et al., "Heavy ion interactions from Coulomb barrier to few GeV/n: Boltzmann master equation theory and FLUKA code performances," *Brazilian J. Phys.*, vol. 34, no. 3, pp. 897–900, Sep. 2004.

[25] H. Aiginger et al., "The FLUKA code: New developments and application to 1 GeV/n iron beams," *Adv. Space Res.*, vol. 35, no. 2, pp. 214–222, Mar. 2005.

[26] V. Andersen et al., "The FLUKA code for space applications: Recent developments," *Adv. Space Res.*, vol. 34, no. 6, pp. 1302–1310, Jan. 2004.

[27] L. Sihver et al., "A comparison of total reaction cross section models used in particle and heavy ion transport codes," *Adv. Space Res.*, vol. 49, no. 4, pp. 812–819, Feb. 2012.

[28] M. Berger, J. Coursey, and M. Zucker. (2005). *ESTAR, PSTAR, and ASTAR: Computer Programs for Calculating Stopping-Power and Range Tables for Electrons, Protons, and Helium Ions (Version 1.2.3)*. [Online]. Available: https://physics.nist.gov/Star

[29] C. Zeitlin and C. La Tessa, "The role of nuclear fragmentation in particle therapy and space radiation protection," *Frontiers Oncol.*, vol. 6, p. 65, Mar. 2016.

[30] M. Bernas et al., "Very heavy fission fragments produced in the spallation reaction $^{238}U_{+p}$ at 1 $AGeV$," *Nucl. Phys. A*, vol. 765, nos. 1–2, pp. 197–210, Jan. 2006.

[31] M. V. Ricciardi et al., "Light nuclides produced in the proton-induced spallation of $^{238}$U at 1-GeV," *Phys. Rev. C*, vol. 73, Aug. 2006, Art. no. 014607.

[32] H. Bethe, "Zur Theorie des Durchgangs schneller korpuskularstrahlen durch materie," *Annalen der Physik*, vol. 397, no. 3, pp. 325–400, Jan. 1930.

[33] R. G. Alía et al., "Fragmented high-energy heavy-ion beams for electronics testing," *IEEE Trans. Nucl. Sci.*, vol. 70, no. 4, pp. 486–495, Apr. 2023.

[34] A. de Bibikoff and P. Lamberbourg, "Method for system-level testing of COTS electronic board under high-energy heavy ions," *IEEE Trans. Nucl. Sci.*, vol. 67, no. 10, pp. 2179–2187, Oct. 2020.

[35] *Test Procedures for the Measurement of SEE in Semiconductor Devices from Heavy-Ion Irradiation*, JEDEC Standard JESD57, 1999.

[36] G. Lindström, "Radiation damage in silicon detectors," *Nucl. Instrum. Methods Phys. Res. A, Accel. Spectrom. Detect. Assoc. Equip.*, vol. 512, nos. 1–2, pp. 30–43, Oct. 2003.

[37] M. A. Clemens et al., "The effects of nuclear fragmentation models on single event effect prediction," *IEEE Trans. Nucl. Sci.*, vol. 56, no. 6, pp. 3158–3164, Dec. 2009.

[38] R. G. Alía et al., "Heavy ion energy deposition and SEE intercomparison within the RADNEXT irradiation facility network," *IEEE Trans. Nucl. Sci.*, vol. 70, no. 8, pp. 1596–1605, Mar. 2023.